Atmos. Meas. Tech. Discuss., 6, 7217–7250, 2013
www.atmos-meas-tech-discuss.net/6/7217/2013/
doi:10.5194/amtd-6-7217-2013


Atmospheric Measurement Techniques Discussions



# Cavity ring-down spectroscopy sensor for detection of hydrogen chloride

**C. L. Hagen[1,*], B. C. Lee[2], I. S. Franka[1], J. L. Rath[1], T. C. VandenBoer[3], J. M. Roberts[3], S. S. Brown[3], and A. P. Yalin[1]**

[1]Department of Mechanical Engineering, Colorado State University, Fort Collins, Colorado
[2]Department of Physics, Colorado State University, Fort Collins, Colorado
[3]NOAA Earth System Research Laboratory, Boulder, Colorado
[*]now at: Oregon State University-Cascades, Bend, Oregon

Received: 3 July 2013 – Accepted: 17 July 2013 – Published: 6 August 2013

Correspondence to: A. P. Yalin (ayalin@engr.colostate.edu)

Published by Copernicus Publications on behalf of the European Geosciences Union.







## Abstract

A laser-based cavity ring-down spectroscopy (CRDS) sensor for measurement of hydrogen chloride (HCl) has been developed and characterized. The instrument uses light from a distributed-feedback diode laser at 1742 nm coupled to a high finesse optical cavity to make sensitive and quantifiable concentration measurements of HCl based on optical absorption. The instrument has a ($1\sigma$) limit of detection of $< 20$ pptv in 1 min and has high specificity to HCl. The measurement response time to changes in input HCl concentration is $< 15$ s. Validation studies with a previously calibrated permeation tube setup show an accuracy of better than 10 %. The CRDS sensor was preliminarily tested in the field with two other HCl instruments (mist chamber and chemical ionization mass spectrometry), all of which were in broad agreement. The mist chamber and CRDS sensors both showed a 400 pptv plume within 50 pptv agreement. The sensor also allows simultaneous sensitive measurements of water and methane, and minimal hardware modification would allow detection of other near-infrared absorbers.

## 1 Introduction

### 1.1 Role of HCl in the atmosphere

Chemical reactions involving halogen radical species, such as chlorine and bromine atoms and their oxides, significantly influence the composition of the Earth's atmosphere. These species also play important roles in many atmospheric processes including the formation and destruction of ozone. In remote regions of the troposphere, such as the polar boundary layer, halogen species are thought to contribute to the destruction of ozone (Vogt et al., 1996; Simpson et al., 2007). The ozone depletion, along with formation of new oxidizing agents, may ultimately lead to a change in the dominant oxidizing agents. In contrast, in polluted marine boundary layers and in populated coastal regions, halogen species can contribute to ozone formation (Tanaka





AMTD
6, 7217–7250, 2013



et al., 2000; Knipping and Dabdub, 2003). Other atmospheric processes in the marine boundary layer, such as the oxidation of methane (Platt et al., 2004; Allan et al., 2007) and larger hydrocarbons (Jobson et al., 1994), can also be influenced by halogens. The chlorine radical also plays a key role in ozone destruction within the upper stratosphere (Solomon, 1999).

Hydrogen chloride, HCl, is an important reservoir species for active halogens. Studies of composite chlorine emissions indicate that HCl is the dominant gas-phase contributor to the overall chlorine inventory in the lower atmosphere (Graedel and Keene, 1995; Keene et al., 1999). The principal source of HCl in the lower atmosphere is thought to be from acid displacement chemistry on sea spray aerosols in the marine boundary layer, though the extent of the contribution from anthropogenic activity, such as coal burning, is not well understood (McCulloch et al., 1999). Chloride present in sea-salt aerosol generated by wind stress at the ocean surface is converted to HCl by acid-displacement reactions (Keene et al., 2007; Pszenny et al., 2004) and references therein. Typical HCl concentrations in remote marine environments span from tens to hundreds of parts per trillion (Kim et al., 2008), while reaching levels of several parts per billion in coastal urban areas (Maben et al., 1995; Keene et al., 2007). In the upper atmosphere ($>\sim 40$ km), HCl is thought to account for more than 90 % of the total chlorine inventory (Achard et al., 1997). However, estimates of HCl production vary considerably and existing measurements are limited. From an industrial perspective, high-temperature chlorine corrosion via HCl can be a costly problem for combustion and gasification plants (Bjoroey et al., 1996). There remains a strong need for improved measurement techniques for HCl, as we address in the present contribution.

### 1.2 Methods for HCl detection

The understanding of sources and sinks of HCl, as well as the role of HCl in proposed chemical mechanisms, requires suitable HCl measurement techniques with sufficient accuracy, sensitivity, specificity, and time-response. Currently, the available instruments for such studies are rather limited. The original methods for such studies involved bulk





AMTD
6, 7217–7250, 2013



sampling with off-line determination of HCl. One method was to sample gas-phase HCl into a solution using a mist chamber collector and to analyze the solution by high resolution ion chromatography (e.g., Keene et al., 1993; Scheuer et al., 2003). The method is attractive owing to its relative simplicity and reliability, but limitations include relatively low time resolution (typically tens of minutes or more) and potential interfering contributions from other active chlorine species, such as $ClNO_2$, so the measurement is often referred to as HCl* (Keene et al., 1993, 2007).

Another method for HCl detection is chemical ionization mass spectrometry (CIMS) (Roberts et al., 2010; Kim et al., 2008; Veres et al., 2008). The CIMS instruments allow selective, rapid, and sensitive detection of species and are amenable to both ground based and aircraft deployments (Veres et al., 2008). A potential limitation of these techniques is their lack of specificity which depends on the details of the ion chemistry scheme. For example, Marcy et al. have reported interference from water vapor (Marcy et al., 2004). The CIMS systems also require periodic zeroing and calibration. In addition, the need for a sensitive mass spectrometer significantly increases the cost of the technique as compared to optical approaches.

Optical absorption based measurements of HCl using infrared laser sources are also possible. By selecting an absorption line of the target species, i.e. $H^{35}Cl$, which does not have nearby interferences from other atmospheric constituents, optical measurements are species specific. Past work has employed tunable diode lasers in a multi-pass Herriot cell for HCl detection (Webster et al., 1994; Scott et al., 1999). The system was sensitive, species-specific, allowed rapid-time response and was amenable to airborne deployment. In order to access the strongest fundamental vibrational band, the system employed lead salt lasers at 3.4 µm paired with mercury-cadmium-telluride (MCT) detectors, both of which required liquid nitrogen ($LN_2$) cooling.

The present instrument seeks to capitalize on advantages of optical absorption approaches, but employs a near-infrared (NIR) diode laser at 1.74 µm. Use of NIR sources with indium-gallium-arsenide (InGaAs) detectors obviates the need for $LN_2$ cooling thereby providing an important practical advantage. Further, the smaller cell volume





AMTD
6, 7217–7250, 2013



possible in CRDS vs. Herriot cells means our CRDS system uses a flow rate more than 10 times smaller than past Herriot cell work, allowing use of smaller and lower power vacuum pumps. In order to attain high detection sensitivity at 1.74 µm (probing the weaker 2-0 vibrational band), continuous wave cavity ring-down spectroscopy (cw-CRDS) is employed to achieve path lengths significantly longer than those from conventional multi-pass cells. The sensor is constructed from robust, readily available, and relatively inexpensive NIR laser sources and components (similar to those used in the telecom industry), which do not need periodic maintenance. Due to the inherently quantifiable nature of CRDS, the sensor requires infrequent calibration. The overall versatility and specificity of this approach makes it attractive for HCl detection in the troposphere allowing, for example, comparisons against existing instruments which measure sums of active chlorine compounds. Additionally, the CRDS technique offers great potential for a very small and low power consumption instrument. Recently, commercial CRDS HCl sensors have become available, but their design and operational details are not available in the open literature.

The layout of the remainder of the paper is as follows. Section 2 provides a description of the HCl CRDS sensor, including spectral simulation, hardware configuration, and operating details. Section 3 discusses instrument performance including characterizations of sensitivity and time response, validation studies with a calibrated permeation tube, and initial field deployment in parallel with two other instruments. The instrument performance specifications are contrasted against those of the aforementioned Herriot cell approach. Possible improvements to the sensor are also discussed. Finally, conclusions are presented in Sect. 4.

## 2 Instrument description

CRDS is an ultra-sensitive laser-based absorption technique, which may be used to measure trace species in the gas phase (Busch and Busch, 1999; Berden et al., 2000). The technique is seeing growing use in a range of fields including combustion





AMTD
6, 7217–7250, 2013



diagnostics, plasma diagnostics, basic spectroscopic studies, and atmospheric trace gas detection. In the cw-CRDS technique, a high-finesse optical cavity is pumped with a continuous-wave (cw) single-mode narrow-linewidth laser. The laser is scanned over a spectral line of the analyte, and when on resonance with the cavity, significant intracavity power is built up. Once such a resonance is detected with a photodetector after the cavity, an acousto-optic modulator is triggered to quickly extinguish the incoming laser beam. The same photodetector measures the subsequent exponential decay of light leaking out from the cavity, termed a ring down. The time constant of the ring down gives the total loss within the cavity. When the laser is tuned to resonance with the analyte, there will be additional loss, causing a faster decay (ring down). Using known line strength parameters for the specific spectral line, and the change in ring-down time, the species concentration can be calculated, the details of which will be given later in this section.

The specific design of a spectroscopic instrument for absorption measurements is guided by the location and strength of the targeted absorption feature. For our instrument, the R(3) $H^{35}Cl$ line of the (2-0) absorption band (see Fig. 1; Rothman et al., 2009) was chosen due to its relatively high strength, its separation from other atmospheric absorbers, and its accessibility using available near-infrared (NIR) components. The (2-0) band corresponds to molecules changing from their initial vibrational level of $v'' = 0$ (i.e. vibrational ground state) to final level of $v' = 2$ as a photon is absorbed. We have labeled the first 5 P- and R-branch transitions (absorption lines) in Fig. 1. The transitions are labeled by the initial rotational level so, for example, R(3) corresponds to molecules changing from initial level of $J'' = 3$ to final level of $J' = 4$ while P(1) corresponds to molecules changing from $J'' = 1$ to $J' = 0$. There are two nearby lines for each transition corresponding to absorption by the two isotopes $H^{35}Cl$ and $H^{37}Cl$. The absorption line strengths include the isotopic abundances (0.758 for $H^{35}Cl$ and 0.242 for $H^{37}Cl$) so that measured concentrations correspond to the overall HCl population (i.e., both isotopes). The targeted line has also been selected by other researchers for laser absorption measurements of HCl (Ortwein et al., 2010; De Rosa et al., 2001).





AMTD
6, 7217–7250, 2013



Although our selected wavelength of 1742 nm is slightly outside the standard telecommunications bands, nearly all of the needed equipment (laser, fiber optics, mirrors, etc) is available from telecomm suppliers. The fundamental (1-0) vibrational band of HCl, near 3.4 µm, has much stronger line strengths and has been used in Herriot cell approaches, with lead salt lasers, discussed above. It is also possible to access this spectral region using difference-frequency generation (DFG) laser sources (Weibring et al., 2010), but these sources and associated components are more expensive and less commercially developed.

Separation from the absorption lines of other potential interfering molecules is critical to successful optical measurements. We have considered interferences due to expected ambient molecules including: $CH_4$, CO, $CO_2$, HCl, $H_2O$, NO, and $N_2O$. As shown in Fig. 2, we have simulated the absorption spectra in the vicinity of the targeted HCl absorption line. The simulations assume typical ambient species concentrations, spectral parameters from HITRAN, and standard expressions for thermal and collisional line broadening (Rothman et al., 2009). There is a tradeoff of operating pressure in the ring-down cell, and we have examined possible performance at difference pressures. Reducing the pressure tends to narrow the spectral absorption features and improve specificity, but at the cost of reduced signal amplitudes and, at sufficiently low pressure ($\sim 0.05$ bar), can introduce operational challenges with the flow system. An operating cell pressure of 0.1 bar was found to be a reasonable compromise.

The literature contains two slightly differing values for the line strength (cross-section) of the targeted HCl line (R(3) $H^{35}Cl$). The 2008 HITRAN database reports a linestrength of $1.16 \times 10^{-20}$ cm molecule$^{-1}$ for the R(3) $H^{35}Cl$ line, which is based on simulation (Tipping, 1990). More recently, Ortwein et al. experimentally studied the same line and reported it to be $1.25 \times 10^{-20}$ cm molecule$^{-1}$ (Ortwein et al., 2010). For the sensor presented here, the authors have adopted the more recent, and experimental value, from Ortwein et al.

Figure 3 shows the schematic layout of the CRDS system. The light source is a distributed-feedback diode laser (KELD1F5DAAA, NEL Lasers, Saddlebrook, NJ,





AMTD
6, 7217–7250, 2013



USA) in a 14-pin butterfly package with a center wavelength of 1742 nm, linewidth of a few MHz, and 13 mW of output power through a single-mode fiber pigtail. Light from the laser is first sent through a 99–1 % fiber-optic beam splitter. The 99 % leg is used as the main interrogating beam, while the weaker leg is used for the frequency calibration leg. When the system is first run, the 1 % output leg from the fiber splitter is sent through a low-finesse Fabry–Perot etalon (fused silica, 45 mm long, finesse ~ 20), and a photodiode (PDA10CS, Thorlabs, Newton, NJ, USA) monitors the etalon transmission signal. The relative frequency of the laser (as determined by the etalon transmission peaks) is plotted against the voltage sent to the laser controller (LDC-3714C, ILX Lightwave, Bozeman, Montana, USA) and fit to a second order polynomial, which provides a relationship between relative laser frequency and controller voltage for subsequent use. This frequency determination procedure is done automatically in our custom LabVIEW software and takes only a few seconds. Owing to the high stability of the DFB laser, these fit coefficients proved stable over months. In regular operation, the etalon is replaced with a custom reference cell which is a sealed glass vessel containing a high concentration of HCl (~ 0.1 %) in atmospheric pressure air. As the instrument runs, the 1 % leg of the beam splitter is sent through the reference cell, and the photodiode monitors the transmission. Due to the high concentration of HCl in the cell, a strong absorption feature is observed through a path length of only a few cm. The sensor control software finds the peak of this absorption feature and centers the laser scan on the HCl spectral feature, thus ensuring any ambient temperature changes do not cause the laser wavelength to drift away from the desired wavelength.

The 99 % output leg from the fiber splitter is first sent through an aspheric collimation lens (CFC-11X-C, $f$ = 11 mm, Thorlabs, Newton, NJ, USA). The aspheric lens is precisely positioned relative to the beam splitter in order to spatially mode match the beam to the $TEM_{0,0}$ mode of the cavity, which also requires proper separation of the cavity and lens (Kogelnik and Li, 1966). After the collimation package, a polarizer and quarter-wave plate are used in series as an optical isolator, blocking light reflected from the cavity from going back into the laser, which, even in small amounts, causes noticeable in-





AMTD
6, 7217–7250, 2013



stability in the laser. The last element before the high-finesse cavity is the acousto-optic modulator (AOM, ACM-402AA1, IntraAction, Bellwood, IL, USA). When the data acquisition (DAQ) system detects a resonance out of the optical cavity, the computer will turn off the AOM, causing the incoming laser to be rapidly extinguished (time constant of ~ 300 ns). The optical cavity itself is constructed of two high-reflectivity dielectric mirrors (Advanced Thin Films, Boulder, CO, USA), with radii of curvature of 2 m and 1 m, and a separation of 90 cm. The mirror reflectivity was determined to be $R$ = 99.9982 % as measured from empty-cavity ring-down times of ~ 170 µs, which was consistent with manufacturer specification.

Indium Gallium Arsenide (InGaAs) photodiodes are widely used for NIR detection, however, the responsivity of InGaAs diodes drops almost two orders of magnitude at 1742 nm as compared to the peak. Extended wavelength InGaAs diodes, with lower bandgap energies, provide higher responsivity farther into the IR, but the dark current also increases significantly. For detection of our main cavity beam, we employ an extended wavelength InGaAs photodiode (G8421-03, Hamamatsu, San Jose, CA, USA), which is soldered onto a transimpedance amplifier (341-4, Analog Modules, Longwood, FL, USA). The amplifier has an input capacitance matched to the photodiode, a gain adjusted to $2 \times 10^6$ V A$^{-1}$, and a bandwidth of 2 MHz. The bandwidth is approximately 5 times larger than needed in order to not distort the ring-down signals. Using a detector with a higher bandwidth than required results in increased noise, as high-frequency detector dark noise is unnecessarily amplified. Other detector options are discussed in Sect. 4. The cavity detector voltage signal is digitized by a 2.5 MS s$^{-1}$, 14-bit PCI multipurpose DAQ card (PCI-6132, National Instruments, Austin, TX, USA), which also controls the AOM. A second DAQ card (PCI-6321, National Instruments, Austin, TX, USA) is used to output the analog voltage signal to the laser controller, as well as to digitize the reference cell detector signal.

A custom LabVIEW program is used to control the instrument and to handle data acquisition and processing. First the software sends an analog voltage to the laser controller, continuously scanning it between 5739.22 and 5739.30 cm$^{-1}$ (as guided by





AMTD
6, 7217–7250, 2013



the reference cell) with a 1 s period triangle wave. When the photodetector signal out of the cavity exceeds a pre-determined threshold (indicative of the laser being in resonance with the cavity), the LabVIEW software turns off the AOM, digitizes the ring-down signal, and fits the data to an exponential function using an iterative non-linear least squares fit seeded by a linear least-squares fit (Lehmann and Huang, 2008). Whenever a ring-down event is recorded, the relative laser frequency is calculated from the etalon calibration. The total DAQ system is capable of acquiring more than 200 ring-downs per second, which is faster than needed, as the system is optically limited to about ~ 25 per second. Once the ring-down time is found, it is converted to an absorption coefficient, $k$, which still includes the empty-cavity loss, given by

$$k = \frac{1}{c\tau}, \tag{1}$$

where $c$ is the speed of light, and $\tau$ is the ring-down time. The LabVIEW software collects ring-down signals for a set amount of time (typically 30 s), termed the integration time, after which the spectrum of recorded absorption values are fit to a Voigt profile, as shown in Fig. 4. The amplitude of the needed frequency scan can change based on the HCl concentration present. For relatively high concentrations, the frequency scan must be wider in order to capture sufficient baseline, such as in Fig. 4. Curve fitting to a Voigt profile can be computationally expensive. To avoid computer downtime, a table of pre-computed Voigt profiles is used. In the current implementation, Voigt and Lorentzian spectral widths are calculated from the known gas conditions inside the sampling cell and used to look up the numerical Voigt profile from the table. The amplitude and offset of these numerical values are then scaled to achieve a linear least-squares fit to the data, and ultimately find the area under the Voigt curve. The measured area under the spectral line, along with the pressure, temperature, and line strength, are used in conjunction with the ideal gas law and the Beer–Lambert law to find the HCl concentration, which is given by

$$[\mathrm{HCl}] = 10^6 \frac{T k_\mathrm{B} A}{P S L_\mathrm{s}}, \tag{2}$$





AMTD
6, 7217–7250, 2013



where $T$ is the temperature of the intra-cavity gas in K, $P$ is the pressure in Pa, $k_B$ is Boltzmann's constant in $JK^{-1}$, $A$ is the area under the spectral line in $cm^{-1}$ (discussed below), $S$ is the line strength in $cm\,molecule^{-1}$, and $L_s$ is the sample path length in cm. The area under the spectral line, $A$, is the integral of the dimensionless cavity loss $\left(\frac{L}{c\tau}\right)$ over frequency in $cm^{-1}$, where $L$ is the cavity length. For CRDS systems in which the interrogated sample fills the entire region between the mirrors, the sample path length is the same as the physical distance between the cavity mirrors. However, as can be seen in Fig. 3, the cavity inlet and outlet flows are connected over a shorter path than the mirror separation distance. A nitrogen purge (flow rate of 0.4 slpm) is introduced in the cavity at each mirror surface in order to prevent particles from contaminating the mirror surfaces, as well as to prevent HCl from potentially interacting with non-Teflon surfaces, where they would strongly adsorb (more details given below). To compensate for the diluted sample, a sample path length replaces the cavity length in Eq. (2) (Brown et al., 2000). To determine the sample path length, the laser wavelength was tuned to the nearby water absorption line in Fig. 2, and the area of this spectral line was found with the purge flow on and off. The cavity length (mirror separation) was multiplied by the ratio of these areas, yielding a sample path length of 86 % of the cavity length (which nearly matches the length between the sample inlet and outlet ports).

Details of the flow system are shown in Fig. 5. As previously mentioned, the system is run at 0.1 bar to ensure separation between spectral features. A vacuum was pulled on the system by a dry scroll pump (IDP2B01, Varian), which provides 8 slpm (including the 0.4 slpm purge flow) of flow through the cavity. Cavity pressure and flow rate were regulated by a combination of two needle valves: a Teflon valve just after the intake and a metal valve on the bypass leg.

The system also employs a simple virtual impactor to remove large particles from the main sampling flow. Not only are large particles in the sample flow threatening to the highly reflective mirror surfaces, but they can scatter or absorb intra-cavity light, increasing the variance in the ring-down time. It is strongly preferred not to use an in-line particulate filter owing to possible measurement artifacts associated with HCl





AMTD
6, 7217–7250, 2013



condensation on to the filter, and aerosol loading and pH-dependent acid-displacement reactions. Instead, the virtual impactor acts as a particle filter by requiring the flow to quickly turn 180 degrees before being routed to the cavity. The design requires the flow to be split into two legs as shown in Fig. 5.

Due to its very high aqueous solubility, HCl has a high propensity to adsorb to surfaces, which constrains the instrument design and limits the detection time response. The adsorption can be partially mitigated by reducing the surface area of the flow system and cavity, and by using Teflon components. Perfluoroalkoxy (PFA), a type of Teflon, was the fluoropolymer of choice because components can be injection molded from PFA resulting in less porous surfaces than other fluoropolymer pieces forged from a powder, such as polytetrafluoroethylene (PTFE). Additionally, the inlet and cavity tubing are heated to 60 °C, which causes surface desorption of the HCl to occur faster, and reduces the amount of moisture available to trap HCl. It has been shown that even using short lengths of extruded nonporous fluoropolymer tubing will adsorb HCl resulting in an instrument response time of greater than 90 s (Roberts et al., 2010). The time response of the present instrument is discussed in Sect. 3.3.

## 3 Sensor performance

This section discusses validation studies and performance metrics for the HCl sensor. The various subsections address the sensor sensitivity (to HCl concentration as well as base optical sensitivity), validation data from a calibrated source, sensor response time, initial field deployment, and potential improvements.

### 3.1 Sensitivity and detection limit

The detection limit of a CRDS sensor for measuring concentrations of trace atmospheric species depends on the instrument's optical precision as well as the spectroscopic relation between the optical absorption and species concentration. We first dis-





AMTD
6, 7217–7250, 2013



cuss the instrument's detection limits in terms of gas concentration measurements after which the optical sensitivity is discussed. While longer integration times generally lead to improved detection limits, eventually system drift dominates such that there is a finite, optimum, integration time. In order to find the ideal integration (averaging) time for the presented CRDS system, we performed an Allan Variance study on a time-sequence of concentration measurements using a modified method (Huang and Lehmann, 2010). The modified method yields a much smoother Allan Variance curve than the traditional two-sample variance method. Figure 6 (top plot) shows a sample concentration data set with the optical cavity purged with ultra-zero air (purity ~ 99.9997 %). The minimum in the Allan Variance is ~ 8 pptv (bottom plot), which occurs at an optimal integration time of ~15 min. For shorter measurement times we find detection limits ($1\sigma$) of 10 pptv after 5 min and ~ 40 pptv after 10 s, where the latter is inferred from the ring-down time data. These values compare favorably against the typical atmospheric abundances that the sensor is designed to measure (see Sect. 1.2). The detection limits of the present instrument are somewhat better than that of past work using MIR lasers and Herriot cells (~ 100 pptv in 30 s; Scott et al., 1999) with the essential difference being that the current sensor has several orders of magnitude better optical sensitivity (owing to our use of CRDS vs. multi-pass cells), but probes weaker lines (2-0 band as opposed to 1-0 band).

We have followed a similar approach to characterize the optical sensitivity of the instrument (independent of analyte). An Allan Variance study of the ring-down times was performed again with ultra-zero air, and is shown in Fig. 7. The minimum in the Allan Variance of ~ 0.01 µs (bottom plot), which occurs at an optimal integration time of ~ 30 s, divided by the mean ring-down time, gives $\left(\frac{\Delta\tau}{\tau}\right)_{\mathrm{Min}}$ of $5.3\times10^{-5}$, where $\left(\frac{\Delta\tau}{\tau}\right)_{\mathrm{Min}}$ is the minimum measurable fractional change in the ring-down time (typically limited by technical noise). Following standard expressions (Zalicki and Zare, 1995), and using $R = 0.99982$ and $L = 90$ cm, results in an optical sensitivity ($1\sigma$) of $1.1\times10^{-11}$ cm$^{-1}$ in 30 s ($6.0\times10^{-11}$ cm$^{-1}$Hz$^{-\frac{1}{2}}$). This optical sensitivity compares favorably against those achieved by other cw-CRDS systems (Berden et al., 2000; Paldus and Kachanov,





AMTD
6, 7217–7250, 2013



2005). From the HITRAN spectral simulations discussed earlier, an optical sensitivity of $1.1 \times 10^{-11}$ cm$^{-1}$ corresponds to a theoretical HCl detection limit of ~ 10 pptv (both for 30 s). This inferred concentration detection limit is a factor of ~ 2–3 better than that actually found for this instrument. The discrepancy is because the laser must be scanned over the broadened spectral line, owing to practical considerations such as drifting cavity loss and laser frequency. The scanning approach captures the baseline on either side of the absorption feature (useful for reliable fitting), but at the cost of lower detection sensitivity. The concentration limit inferred from the ring downs would apply if the laser were fixed at a single frequency on the spectral line peak.

### 3.2 HCl validation data

We have performed tests with an HCl calibration source in order to validate the accuracy of the instrument. Such characterizations are particularly important for gas phase HCl because it is a difficult molecule to sample due to adsorption (see end of Sect. 2). The validation source uses a permeation tube containing hydrochloric acid, which slowly diffuses through the Teflon tube wall. The tube emits gaseous HCl at a rate of $10 \pm 1$ ng min$^{-1}$ when temperature controlled at 55 °C. The emission rate was characterized by comparison with a 10 ppmv gaseous HCl standard. The 10 ppmv standard was cross checked by conversion to HONO and measurement by incoherent broadband cavity-enhanced absorption spectroscopy and total $NO_y$ (Roberts et al., 2010). Ultra-pure zero air (Airgas, 99.9997 % pure) flows over the permeation tube at a rate of 9.9 sccm, giving an HCl concentration of 630 ppbv. The flow from the permeation tube is further diluted by a few slpm of zero air at a rate set by an adjustable mass flow controller, thereby allowing the final HCl concentration to be set. Finally, the calibration air is sent into the inlet of the system.

Figure 8 shows concentration data measured by the CRDS instrument plotted against the input concentration. A range of HCl concentrations, between 0.75 and 6.25 ppbv, from the calibration source were studied. Each plotted point is a 10 min average (corresponding to averaging 20 measurements each obtained over 30 s), and





AMTD
6, 7217–7250, 2013



the red line shows the ideal 1 : 1 correlation. The errors bars in the input concentrations are due to a 10 % uncertainty in the calibration source, while errors bars on the measured concentration are taken as the (1 $\sigma$) standard deviation in the measured values during the 10 min averaging time. We do not see any obvious systematic error, for example as would be the case if the assumed linestrength were incorrect, and we observe consistency of better than 10 % between the expected and measured values, similar to that reported in past work using lead salt lasers and Herriot cells (Scott et al., 1999).

### 3.3 Response time

A potential advantage of using optical approaches for HCl measurement is the ability to have relatively fast instrument response times. Of course, instrument temporal response also determines utility for field campaigns, especially those using mobile platforms. Because HCl has high aqueous solubility and strongly adsorbs onto surfaces, the inlet design and sensor time response are particularly challenging. Past work has shown that designing a fast-response inlet and flow system for HCl is difficult and requires careful consideration of flow-rates, materials, and geometry (Roberts et al., 2010).

Using a similar setup as that described in the above subsection (but with a different permeation tube), we characterized the response time for several inlet and flow-system designs. We provided step-changes in the input concentration and characterized the response time based on the time needed to reach 90 % of the (step change of the) final settled value. Figure 9 shows an example of a time-sequence of raw ring-down times during a step change in HCl concentration (ppbv level) yielding a 90 % settling time of 10 s. Ring-down times at the HCl absorption peak center are used, as they are directly responsive to changes in HCl concentration. While these values do not give absolute HCl concentrations without capturing the spectral baseline, they provide a fast measurement update rate, which is needed for such response time studies. The HCl settling time in our final design, which uses a PFA Teflon cavity of 6.4 mm inner





AMTD
6, 7217–7250, 2013



diameter and flow rate of 8 slpm, is consistently below 30 s. The cavity was held at 60 °C with resistive heaters. This response time is likely limited by gas adsorption effects since similar characterizations, based on changes in $CO_2$ concentration (and using the spectrally close $CO_2$ feature), yielded response times of < 1 s consistent with the transit time (residence time) of gas in our cavity.

A series of experiments were conducted to better understand the factors influencing the response time. In all cases, the optical cavity and inlet tubing were made from PFA Teflon owing to its low porosity. While keeping other conditions fixed, we studied response times for optical cavities of inner-diameters 9.5, 7.9, and 6.4 mm and found that the response time was fairly linear against diameter (i.e., cavity surface area). Significant reductions to even smaller diameters are not possible owing to the mode-matched beam dimensions within the cavity. We have also studied the response time for gas flow rates of 3, 4, 5, and 7 slpm through the system and found the response time scales as roughly inverse of the flow-rate. This finding is consistent with earlier work showing that the HCl measurement settling time can be related to the number of residence times of the gas in the sensor and that approximately 30–60 residence times are needed for HCl (Fried et al., 1984).

### 3.4 Field study demonstration

The first field test of the present CRDS instrument was during the Nitrogen, Aerosol Composition and Halogens on a tall tower (NACHTT) campaign, in Weld County, Colorado during early 2011(Brown et al., 2013). Although the instrument was still early in its development, the field campaign provided an opportunity to run our instrument side-by-side with two other instruments employing different HCl measurement methods. The first method being acid CIMS (VandenBoer et al., 2013), and the second method being mist chamber ion-chromatography (Young et al., 2013).

Located within a box truck, the CRDS instrument collected air samples from the base of the Boulder Atmospheric Observatory, a 300 m research tower. The mist chamber ion-chromatography instrument was also located at the tower base with an inlet 22 m





AMTD
6, 7217–7250, 2013



a.g.l., while the acid CIMS instrument traveled in a carriage up and down the tower. HCl concentration measurements taken by the three HCl instruments are compared in Fig. 10. The sample data set, taken around 21:30 MST on Day 21 (17 February 2011) of the study, shows agreement between the three instruments, including observation of a plume containing ~ 400 pptv of HCl within ~ 50 pptv agreement. At the time of the NACHTT study, the optical precision of the sensor was a factor of ~ 5 poorer than the current instrument, since many improvements were made subsequently.

### 3.5 Instrument improvements

In the remainder of this Sect., possible instrument modifications are briefly discussed. While these modifications may improve performance, we note the current performance is very adequate for most field study needs. From an optical point of view, several improvements could be considered. First, a detector and amplifier combination with somewhat lower bandwidth (~ 400 kHz) would allow faithful measurement of the ring-down signal while lowering the adverse effects of high-frequency noise. Second, a thermo-electrically cooled photodiode could be used to reduce the detector dark noise. Further, improved sensitivity can be obtained from more complicated CRDS schemes, though at the cost of increased hardware cost and complexity. One such example is to use a Pound–Drever–Hall locked cavity similar to Spence et al. (2000) where the laser and cavity frequencies are locked together such that higher ring-down acquisition rates of several kHz are possible. It would be reasonable to expect a factor of ~ 5 or more improvement in detection limit by implementing this technique into the presented instrument.

From a packaging point of view, a more compact and robust design would be attractive for studies on aircraft or boats. The overall dimensions of the CRDS instrument are ~ 1.4 × 1.2 × 0.55 m. Currently, a commercial optical breadboard is used to mount all of the optical components while a straightforward improvement would be to use a smaller dedicated breadboard that could be mounted on a spring-damping system for improved vibration isolation. Further, the data acquisition computer uses a relatively





AMTD
6, 7217–7250, 2013



large PCI DAQ card, which could be replaced with a smaller and faster PCIe card. Issues related to the sticky gas adsorption can also be further investigated, with the goal of reducing the settling time, such as possible sample line passivation procedures (Keene et al., 1993).

Finally, as can be seen in Fig. 2, the current system can readily detect nearby spectral absorption lines due to water and methane. While these lines are not optimum selections for these molecules, they could be detected concurrently with HCl with detection limits of ~ 5 ppmv and ~ 2 ppbv for water and methane respectively (based on scaling the HCl data by relative linestrengths). Additionally, by changing only the laser, cavity mirrors, and quarter-wave plate, other NIR absorbing molecules such as CO, $CO_2$, and $H_2S$ would be readily measurable.

## 4 Conclusions

This contribution has described the design and characterization of an HCl sensor utilizing cw-CRDS. Relatively low-cost NIR components, similar to those used in telecommunications, were used to create the instrument. The instrument features HCl detection limits of < 20 pptv in 1 min with optimum integration times of ~ 15 min to achieve the best possible detection limit of 8 pptv. Calibration studies have shown good agreement with expected values (accuracy better than ~ 10 %). We also find (90 % settling) response times of < 15 s for step-changes in input concentration.

The instrument performance metrics should meet the needs for many measurement campaigns and compares favorably against other instruments. For example, there is interest in deploying such sensors on future aircraft campaigns. With a 10 s measurement time, the sensor provides a limit of detection ($1\sigma$) of ~ 40 pptv, which should be sufficient for HCl measurements near coastal areas. Assuming a typical aircraft cruising speed of 100 m s$^{-1}$, HCl concentrations could be made with a ~ 1 km spatial resolution.

Relative to the past work with Herriott cells, the present instrument does not require $LN_2$ cooled lead salt lasers or detectors (though DFG lasers, with Herriot cells, may





AMTD
6, 7217–7250, 2013



also be of future interest). And, for measurements of sticky gases, the larger surface area of Herriot cells (as well as off-axis cavity enhanced cells) is challenging for time response unless much higher flow rates (larger pumps) are used. While there is at least one commercial CRDS instrument available for HCl, the details of its spectroscopy and design are not in the open literature, which can be particularly important for use in field studies where it may be needed to reconfigure the inlet to achieve tradeoffs in flow-rate, response time etc. A prototype of the present instrument was demonstrated in a field campaign, showing consistency against other HCl instruments.

*Acknowledgements.* The authors acknowledge A. A. P. Pszenny and W. C. Keene for their permission to present data from their mist chamber ion-chromatography instrument. Finally, the authors also acknowledge funding support from the National Science Foundation (Award Number: 0948015).

## References

Achard, V., De Mazière, M., Camy-Peyret, C., Karcher, F., and Lippens, C.: Spaceborne measurements of the upper stratospheric HCl vertical distribution in early 1992 and the trend in total stratospheric chlorine since 1985, J. Geophys. Res.-Atmos., 102, 8985–8990, doi:10.1029/97JD00004, 1997. 7219

Allan, W., Struthers, H., and Lowe, D. C.: Methane carbon isotope effects caused by atomic chlorine in the marine boundary layer: global model results compared with Southern Hemisphere measurements, J. Geophys. Res., 112, D04306, doi:10.1029/2006JD007369, 2007. 7219

Berden, G., Peeters, R., and Meijer, G.: Cavity ring-down spectroscopy: experimental schemes and applications, Int. Rev. Phys. Chem., 19, 565–607, doi:10.1080/014423500750040627, 2000. 7221, 7229

Bjoroey, O., Haugholt, K. H., and Jaeger, T.: Diode laser spectroscopy of gaseous HCl, Quantum Electron., 26, 1090–1092, 1996. 7219

Brown, S. S., Wilson, R. W., and Ravishankara, A. R.: Absolute intensities for third and fourth overtone absorptions in $HNO_3$ and $H_2O_2$ measured by cavity ring down spectroscopy, J. Phys. Chem. A, 104, 4976–4983, doi:10.1021/jp000439d, 2000. 7227





AMTD
6, 7217–7250, 2013



Brown, S. S., Thornton, J. A., Keene, W. C., Pszenny, A. A. P., Sive, B. C., Dubé, W. P., Wagner, N. L., Young, C. J., Riedel, T. P., Roberts, J. M., VandenBoer, T. C., Bahreini, R., Öztürk, F., Middlebrook, A. M., Kim, S., Hübler, G., and Wolfe, D. E.: Nitrogen, Aerosol Composition and Halogens on a Tall Tower (NACHTT): overview of a wintertime air chemistry field study in the front range urban corridor of Colorado, J. Geophys. Res.-A., doi:10.1002/jgrd.50537, in press, 2013. 7232

Busch, K. and Busch, M.: Cavity-Ringdown Spectroscopy (ACS Symposium Series 720), Oxford University Press, 1999. 7221

De Rosa, M., Nardini, C., Piccolo, C., Corsi, C., and D'Amato, F.: Pressure broadening and shift of transitions of the first overtone of HCl, Appl. Phys. B-Lasers-O, 72, 245–248, doi:10.1007/s003400000449, 2001. 7222

Fried, A., Sams, R., and Berg, W. W.: Application of tunable diode laser absorption for trace stratospheric measurements of HCl: laboratory results, Appl. Optics, 23, 1867–1880, doi:10.1364/AO.23.001867, 1984. 7232

Graedel, T. E. and Keene, W. C.: Tropospheric budget of reactive chlorine, Global Biogeochem. Cy., 9, 47–77, 1995. 7219

Huang, H. and Lehmann, K. K.: Long-term stability in continuous wave cavity ringdown spectroscopy experiments, Appl. Optics, 49, 1378–1387, doi:10.1364/AO.49.001378, 2010. 7229

Jobson, B. T., Niki, H., Yokouchi, Y., Bottenheim, J., Hopper, F., and Leaitch, R.: Measurements of $C_2$-$C_6$ hydrocarbons during the Polar sunrise 1992 experiment: evidence for Cl atom and Br atom chemistry, J. Geophys. Res.-Atmos., 99, 25355–25368, doi:10.1029/94JD01243, 1994. 7219

Keene, W., Stutz, J., Pszenny, A. A. P., Maben, J. R., Fischer, E. V., Smith, A. M., von Glasow, R., Pechtl, S., Sive, B. C., and Varner, R. K.: Inorganic chlorine and bromine in coastal New England air during summer, J. Geophys. Res., 112, D10S12, doi:10.1029/2006JD007689, 2007. 7219, 7220

Keene, W. C., Maben, J. R., Pszenny, A. A. P., and Galloway, J. N.: Measurement technique for inorganic chlorine gases in the marine boundary-layer, Environ. Sci. Technol., 27, 866–874, doi:10.1021/es00042a008, 1993. 7220, 7234

Keene, W. C., Khalil, M. A. K., Erickson, D. J., McCulloch, A., Graedel, T. E., Lobert, J. M., Aucott, M. L., Gong, S. L., Harper, D. B., Kleiman, G., Midgley, P., Moore, R. M., Seuzaret, C., Sturges, W. T., Benkovitz, C. M., Koropalov, V., Barrie, L. A., and Li, Y. F.: Composite global emissions of reactive chlorine from anthropogenic and natural





AMTD
6, 7217–7250, 2013



sources: Reactive Chlorine Emissions Inventory, J. Geophys. Res.-Atmos., 104, 8429–8440, doi:10.1029/1998JD100084, 1999. 7219

Kim, S., Huey, L. G., Stickel, R. E., Pierce, R. B., Chen, G., Avery, M. A., Dibb, J. E., Diskin, G. S., Sachse, G. W., McNaughton, C. S., Clarke, A. D., Anderson, B. E., and Blake, D. R.: Airborne measurements of HCl from the marine boundary layer to the lower stratosphere over the North Pacific Ocean during INTEX-B, Atmos. Chem. Phys. Discuss., 8, 3563–3595, doi:10.5194/acpd-8-3563-2008, 2008. 7219, 7220

Knipping, E. M. and Dabdub, D.: Impact of chlorine emissions from sea-salt aerosol on coastal urban ozone, Environ. Sci. Technol., 37, 275–284, 2003. 7219

Kogelnik, H. and Li, T.: Laser beams and resonators, Appl. Optics, 5, 1550–1567, doi:10.1364/AO.5.001550, 1966. 7224

Lehmann, K. and Huang, H.: Frontiers of Molecular Spectroscopy, in: Optimal signal processing in cavity ring-down spectroscopy, edited by: Laane, J., Elsevier, 2008. 7226

Maben, J. R., Keene, W. C., Pszenny, A. A. P., and Galloway, J. N.: Volatile inorganic Cl in surface air over eastern North America, Geophys. Res. Lett., 22, 3513–3516, doi:10.1029/95GL03335, 1995. 7219

Marcy, T. P., Fahey, D. W., Gao, R. S., Popp, P. J., Richard, E. C., Thompson, T. L., Rosenlof, K. H., Ray, E. A., Salawitch, R. J., Atherton, C. S., Bergmann, D. J., Ridley, B. A., Weinheimer, A. J., Loewenstein, M., Weinstock, E. M., and Mahoney, M. J.: Quantifying stratospheric ozone in the upper troposphere with in situ measurements of HCl, Science, 304, 261–263, 2004. 7220

McCulloch, A., Aucott, M. L., Benkovitz, C. M., Graedel, T. E., Kleiman, G., Midgley, P. M., and Li, Y.-F.: Global emissions of hydrogen chloride and chloromethane from coal combustion, incineration and industrial activities: reactive chlorine emissions inventory, J. Geophys. Res.-Atmos., 104, 8391–8403, doi:10.1029/1999JD900025, 1999. 7219

Ortwein, P., Woiwode, W., Wagner, S., Gisi, M., and Ebert, V.: Laser-based measurements of line strength, self- and pressure-broadening coefficients of the $H^{35}Cl$ R(3) absorption line in the first overtone region for pressures up to 1 MPa, Appl. Phys. B-Lasers-O, 100, 341–347, doi:10.1007/s00340-009-3862-8, 2010. 7222, 7223

Paldus, B. and Kachanov, A.: An historical overview of cavity enhanced methods, Can. J. Phys., 83, 975–999, 2005. 7229





AMTD
6, 7217–7250, 2013



Platt, U., Allan, W., and Lowe, D.: Hemispheric average Cl atom concentration from $^{13}C^{12}C$ ratios in atmospheric methane, Atmos. Chem. Phys., 4, 2393–2399, doi:10.5194/acp-4-2393-2004, 2004. 7219

Pszenny, A. A. P., Moldanová, J., Keene, W. C., Sander, R., Maben, J. R., Martinez, M., Crutzen, P. J., Perner, D., and Prinn, R. G.: Halogen cycling and aerosol pH in the Hawaiian marine boundary layer, Atmos. Chem. Phys., 4, 147–168, doi:10.5194/acp-4-147-2004, 2004. 7219

Roberts, J. M., Veres, P., Warneke, C., Neuman, J. A., Washenfelder, R. A., Brown, S. S., Baasandorj, M., Burkholder, J. B., Burling, I. R., Johnson, T. J., Yokelson, R. J., and de Gouw, J.: Measurement of HONO, HNCO, and other inorganic acids by negative-ion proton-transfer chemical-ionization mass spectrometry (NI-PT-CIMS): application to biomass burning emissions, Atmos. Meas. Tech., 3, 981–990, doi:10.5194/amt-3-981-2010, 2010. 7220, 7228, 7230, 7231

Rothman, L. S., Gordon, I. E., Barbe, A., Benner, D. C., Bernath, P. F., Birk, M., Boudon, V., Brown, L. R., Campargue, A., Champion, J.-P., Chance, K., Coudert, L. H., Dana, V., Devi, V. M., Fally, S., Flaud, J.-M., Gamache, R. R., Goldman, A., Jacquemart, D., Kleiner, I., Lacome, N., Lafferty, W. J., Mandin, J.-Y., Massie, S. T., Mikhailenko, S. N., Miller, C. E., Moazzen-Ahmadi, N., Naumenko, O. V., Nikitin, A. V., Orphal, J., Perevalov, V. I., Perrin, A., Predoi-Cross, A., Rinsland, C. P., Rotger, M., Šimečkovă, M., Smith, M. A. H., Sung, K., Tashkun, S. A., Tennyson, J., Toth, R. A., Vandaele, A. C., and Vander Auwera, J.: The HITRAN 2008 molecular spectroscopic database, J. Quant. Spectrosc. Ra., 110, 533–572, doi:10.1016/j.jqsrt.2009.02.013, 2009. 7222, 7223

Scheuer, E., Talbot, R. W., Dibb, J. E., Seid, G. K., DeBell, L., and Lefer, B.: Seasonal distributions of fine aerosol sulfate in the North American Arctic basin during TOPSE, J. Geophys. Res., 108, 8370, doi:10.1029/2001JD001364, 2003.

Scott, D. C., Herman, R. L., Webster, C. R., May, R. D., Flesch, G. J., and Moyer, E. J.: Airborne Laser Infrared Absorption Spectrometer (ALIAS-II) for in situ atmospheric measurements of $N_2O$, $CH_4$, CO, HCl, and $NO_2$ from balloon or remotely piloted aircraft platforms, Appl. Optics, 38, 4609–4622, 1999. 7220, 7229, 7231

Simpson, W. R., von Glasow, R., Riedel, K., Anderson, P., Ariya, P., Bottenheim, J., Burrows, J., Carpenter, L. J., Frieß, U., Goodsite, M. E., Heard, D., Hutterli, M., Jacobi, H.-W., Kaleschke, L., Neff, B., Plane, J., Platt, U., Richter, A., Roscoe, H., Sander, R., Shepson, P., Sodeau, J., Steffen, A., Wagner, T., and Wolff, E.: Halogens and their role in polar boundary-





AMTD
6, 7217–7250, 2013



layer ozone depletion, Atmos. Chem. Phys., 7, 4375–4418, doi:10.5194/acp-7-4375-2007, 2007. 7218
Solomon, S.: Stratospheric ozone depletion: a review of concepts and history, Rev. Geophys., 37, 275–316, 1999. 7219
Spence, T. G., Harb, C. C., Paldus, B. A., Zare, R. N., Willke, B., and Byer, R. L.: A laser-locked cavity ring-down spectrometer employing an analog detection scheme, Rev. Sci. Instrum., 71, 347–353, doi:10.1063/1.1150206, 2000. 7233
Tanaka, P. L., Oldfield, S., Neece, J. D., Mullins, C. B., and Allen, D. T.: Anthropogenic sources of chlorine and ozone formation in urban atmospheres, Environ. Sci. Technol., 34, 4470–4473, 2000. 7218
Tipping, R.: Calculation of Spectroscopic Parameters for Diatomic Molecules of Atmospheric Interest, Defense Technical Information Center, Alabama University, 1990. 7223
VandenBoer, T. C., Brown, S. S., Murphy, J. G., Keene, W. C., Young, C. J., Pszenny, A. A. P., Kim, S., Warneke, C., de Gouw, J. A., Maben, J. R., Wagner, N. L., Riedel, T. P., Thornton, J. A., Wolfe, D. E., Dubé, W. P., Öztürk, F., Brock, C. A., Grossberg, N., Lefer, B., Lerner, B., Middlebrook, A. M., and Roberts, J. M.: Understanding the role of the ground surface in HONO vertical structure: High resolution vertical profiles during NACHTT-11, J. Geophys. Res., submitted, 2013. 7232
Veres, P., Roberts, J. M., Warneke, C., Welsh-Bon, D., Zahniser, M., Herndon, S., Fall, R., and de Gouw, J.: Development of negative-ion proton-transfer chemical-ionization mass spectrometry (NI-PT-CIMS) for the measurement of gas-phase organic acids in the atmosphere, Int. J. Mass Spectrom., 274, 48–55, doi:10.1016/j.ijms.2008.04.032, 2008. 7220
Vogt, R., Crutzen, P. J., and Sander, R.: A mechanism for halogen release from sea-salt aerosol in the remote marine boundary layer, Nature, 383, 327–329, 1996. 7218
Webster, C. R., May, R. D., Trimble, C. A., Chave, R. G., and Kendall, J.: Aircraft (ER-2) laser infrared absorption spectrometer (ALIAS) for in-situ stratospheric measurements of HCl, $N_2O$, $CH_4$, $NO_2$, and $HNO_3$, Appl. Optics, 33, 454–472, 1994. 7220
Weibring, P., Richter, D., Walega, J. G., Rippe, L., and Fried, A.: Difference frequency generation spectrometer for simultaneous multispecies detection, Opt. Express, 18, 27670–27681, doi:10.1364/OE.18.027670, 2010. 7223
Young, A. H., Keene, W. C., Pszenny, A. A. P., Sander, R., Thornton, J. A., Riedel, T. P., and Maben, J. R.: Phase Partitioning of Soluble Trace Gases with Size-Resolved Aerosols in





AMTD
6, 7217–7250, 2013



Near-Surface Continental Air over Northern Colorado, USA During Winter, J. Geophys. Res., in press, 2013. 7232
Zalicki, P. and Zare, R.: Cavity ring-down spectroscopy for quantitative absorption measurements, J. Chem. Phys., 102, 2708–2717, 1995. 7229





AMTD
6, 7217–7250, 2013



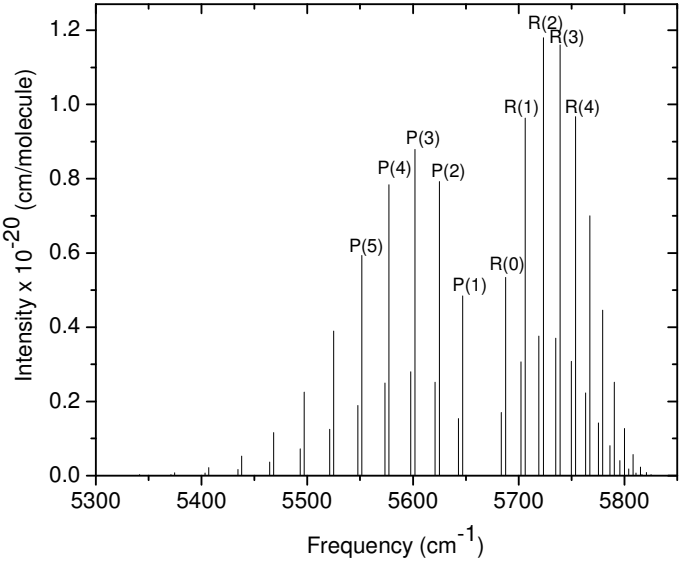


**Fig. 1.** Linestrengths of rotational lines of the 2-0 vibrational absorption band of $H^{35}Cl$ and $H^{37}Cl$ from HITRAN. The CRDS sensor uses the R(3) line of $H^{35}Cl$ at 5739.26 $cm^{-1}$.





AMTD
6, 7217–7250, 2013

Cavity ring-down spectroscopy sensor for detection of hydrogen chloride

C. L. Hagen et al.



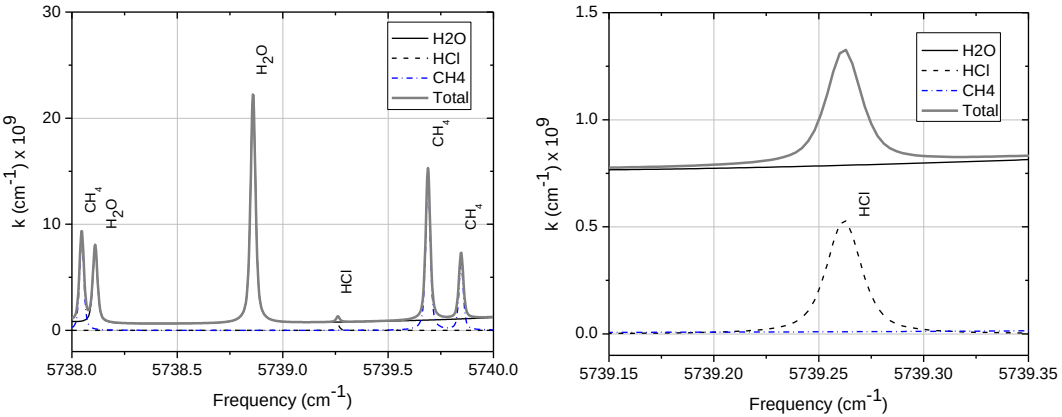


**Fig. 2.** Simulated absorption spectra in the vicinity of the targeted HCl absorption line. Simulated conditions are: $P$ = 0.1 bar, $T$ = 295 K, HCl = 0.5 ppbv, $CH_4$ = 2 ppmv, $H_2O$ = 0.013 (50 % Relative Humidity). Left/right: zoomed out/in of HCl line.





AMTD
6, 7217–7250, 2013

Cavity ring-down spectroscopy sensor for detection of hydrogen chloride

C. L. Hagen et al.



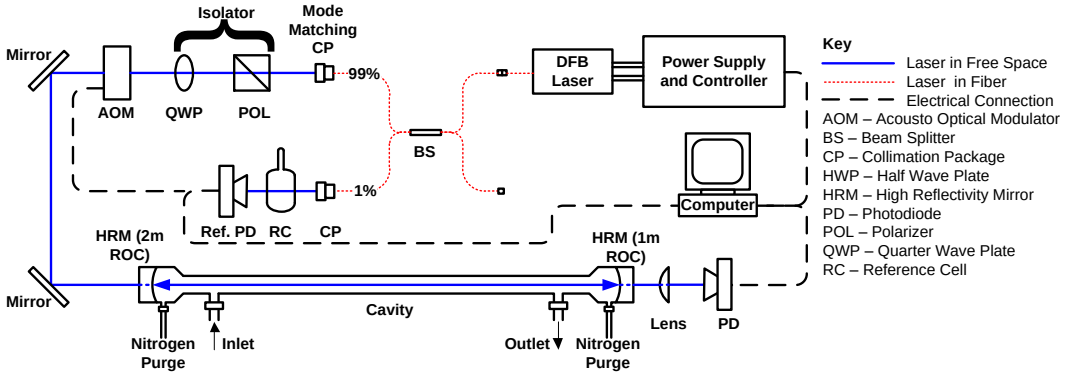


**Fig. 3.** Schematic of the optical components and data acquisition systems of the HCl sensor.





AMTD
6, 7217–7250, 2013



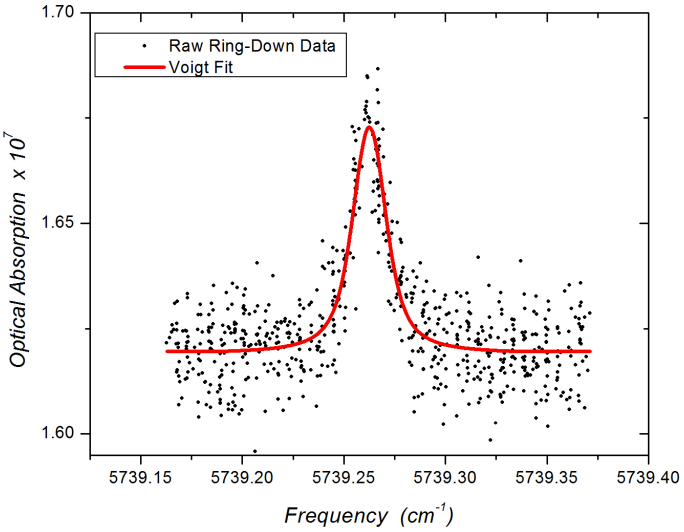


**Fig. 4.** Example plot of the measured dimensionless absorption values vs. frequency in the vicinity of the HCl absorption feature after 30 s of acquisition time. The red line is a Voigt profile fit. The non-zero baseline is due to the cavity mirror loss. The measured HCl concentration in this case is 6.25 ppbv.





AMTD
6, 7217–7250, 2013



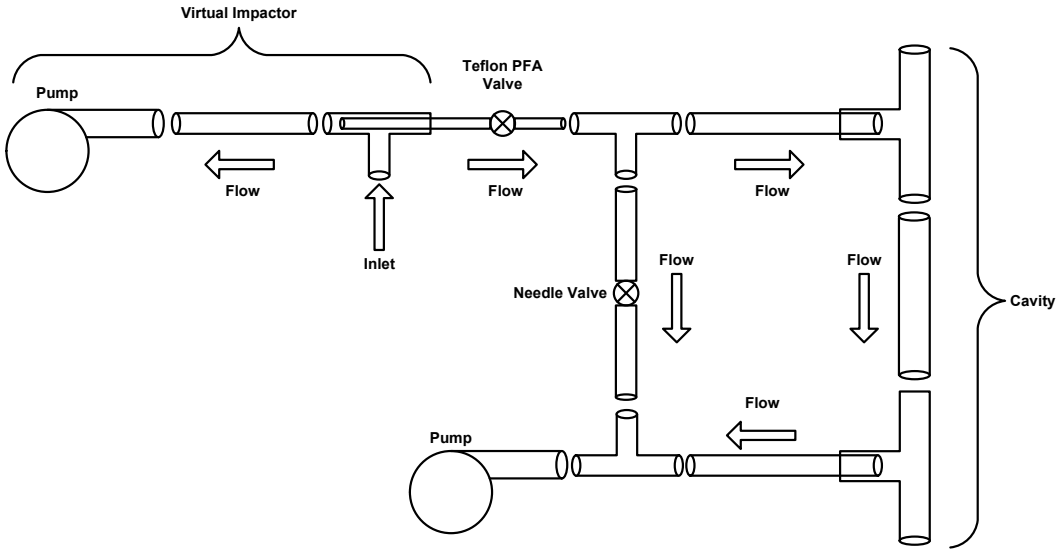


**Fig. 5.** Schematic diagram of the HCl sensor gas flow system. The virtual impactor, indicated on the left, serves to remove large particles from the main sampling flow. The optical cavity is indicated on the right.





AMTD
6, 7217–7250, 2013

Cavity ring-down spectroscopy sensor for detection of hydrogen chloride

C. L. Hagen et al.



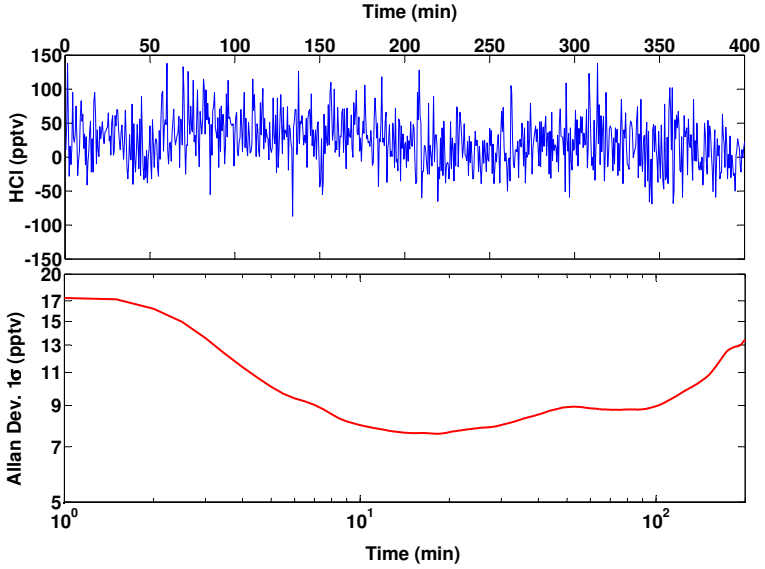


**Fig. 6.** Measured HCl concentration values (top) and their associated Allan Deviation curve (bottom) with the optical cavity purged with ultra-zero air. The measurement period was 30 s.





AMTD
6, 7217–7250, 2013



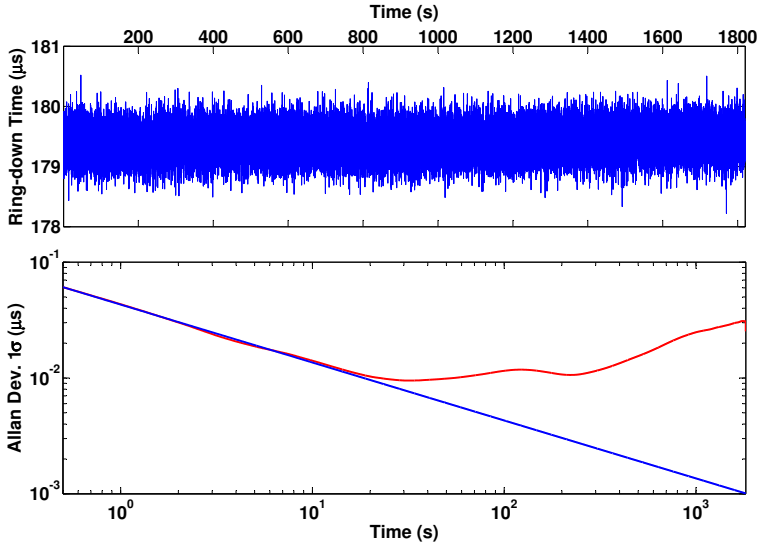


**Fig. 7.** Top: sample ring-down data when the optical cavity was purged with ultra-zero air. Bottom: modified Allan Deviation of the ring-down data (red solid line) as compared to the idealized data without drift, i.e. $t^{-1/2}$ dependence (blue dashed line). The average rate at which ring downs are acquired is ~ 20 Hz, however, it is not constant, as the computer simply triggers whenever a resonance is detected.





AMTD
6, 7217–7250, 2013



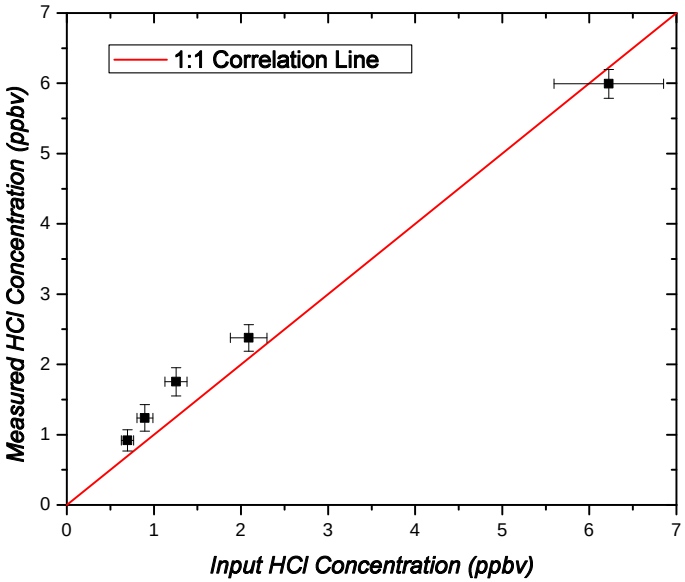


**Fig. 8.** HCl concentration measurements averaged for 10 min as compared to the concentration supplied to the inlet from the calibration system. The solid line shows the expected 1 : 1 correlation between the measured and input values.





AMTD
6, 7217–7250, 2013

Cavity ring-down spectroscopy sensor for detection of hydrogen chloride

C. L. Hagen et al.



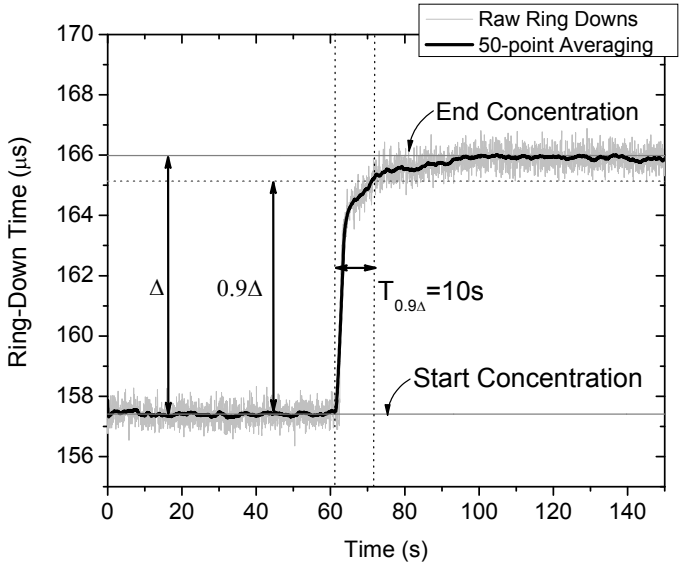


**Fig. 9.** Time sequence of ring-down signals (obtained with laser tuned near HCl peak) as the HCl input concentration was impulsively changed (at $T$ = 20 s). The instrument response time was found as 10 s (based on the time needed to capture 90 % of the final change).





AMTD
6, 7217–7250, 2013

Cavity ring-down spectroscopy sensor for detection of hydrogen chloride

C. L. Hagen et al.



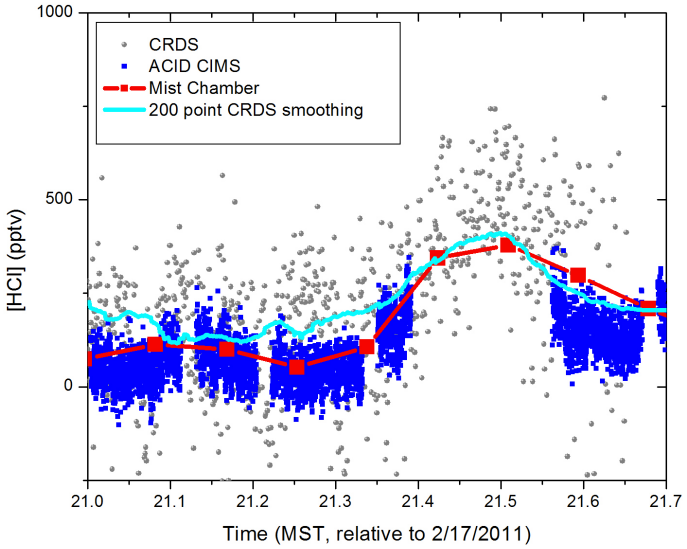


**Fig. 10.** HCl concentration values recorded by the CRDS, ACID CIMS, and mist chamber instruments during the NACHTT campaign.





AMTD
6, 7217–7250, 2013

Cavity ring-down spectroscopy sensor for detection of hydrogen chloride

C. L. Hagen et al.